JOURNAL OF THERMOPHYSICS AND HEAT TRANSFER
Vol. 24, No. 3, July–September 2010

Compressible Laminar Boundary-Layer Flows with Statistical Bhatnagar–Gross–Krook Approaches

Rakesh Kumar,* E. V. Titov,† and D. A. Levin‡
Pennsylvania State University, University Park, Pennsylvania 16802

DOI: 10.2514/1.45699

In this work, we study the well-known, fundamental viscous fluid problem of compressible, laminar boundary-layer flow over a flat plate. The paper investigates the modeling of such flows using the Bhatnagar–Gross–Krook and ellipsoidal statistical Bhatnagar–Gross–Krook model kinetic equations for the supersonic flow of argon gas over a flat plate in the semirarefied regime. The Bhatnagar–Gross–Krook and ellipsoidal statistical Bhatnagar–Gross–Krook solutions are compared with the exact, well-known direct simulation Monte Carlo method as well as the theoretical solution of the boundary-layer equations that include velocity slip and temperature jump boundary conditions for adiabatic and isothermal wall boundary conditions. It is found that the solutions obtained by the statistical Bhatnagar–Gross–Krook and ellipsoidal statistical Bhatnagar–Gross–Krook methods agree well with the theoretical and the benchmark direct simulation Monte Carlo solutions. Both approaches capture the shock wave appearing at the leading edge of the flat plate, but the ellipsoidal statistical Bhatnagar–Gross–Krook approach is shown to be in better agreement with the benchmark direct simulation Monte Carlo method solutions as well as the theoretical results. In addition, the statistical Bhatnagar–Gross–Krook and ellipsoidal statistical Bhatnagar–Gross–Krook methods are shown to be numerically more efficient than the direct simulation Monte Carlo method.

I. Introduction

COMPRESSIBLE boundary-layer problem flow over a flat plate, although well known, is still of great interest because it is present in many practical applications of geometrically complex flows. Chapman and Rubesin [1] studied compressible laminar boundary layer over a flat plate with an arbitrary surface temperature distribution because of its importance to the stability characteristics of the boundary layer. Cecil and McDaniel [2] carried out experimental studies using a flat plate model as part of the development of an aerobraking device. In this work, a simplified flat plate model of a more complex body allowed them to extract the major flow parameters required for the design of the device. Study of compressible boundary-layer flows in the transitional regime has also emerged as an active area of interest in microelectromechanical systems (MEMS). Ho and Tai [3] studied boundary-layer flow through a straight two-dimensional microchannel to examine the surface effects that dominated the flow through these miniature devices. Likewise, Liou and Fang [4] studied low- and high-speed boundary-layer flows through two-dimensional planar microchannels to gain a detailed understanding of the heat transfer in microchannel flows, again using two closely spaced flat plates to model the microchannel. What makes the study of boundary-layer flows especially interesting is that they can be studied theoretically, which in turn allows the corroboration of numerical studies; they are also still relevant to newly developed microscale devices.

Numerical simulation of the boundary-layer flows in the transitional regime has been widely studied using the direct simulation Monte Carlo (DSMC) method, an approach that provides a numerical solution of the Boltzmann equation. The importance of rarefied flow over a flat plate motivated a number of authors [5,6] to solve the boundary-layer flow in the transitional regime by the DSMC method. Padilla and Boyd [5] studied gas–surface interaction models in a compressible flow over a flat plate at a Knudsen number of 0.004. The comparison of their DSMC solutions with continuum boundary-layer theory demonstrated the need for a kinetic approach for such flows to account for rarefied gas effects. Sun and Boyd [6] studied the aerodynamics characteristics of a 5% flat plate airfoil across a range of Reynolds numbers using the DSMC method and showed that the aerodynamic performance of the 5% airfoil is poor at very low Reynolds numbers.

In general, the DSMC method is used in modeling complex physical flows such as thermally and chemically nonequilibrium flows [7,8], multiphase flows [9], and radiative flows [10,11]. However, the method becomes increasingly computationally expensive when the flow regime is close to continuum, which often renders the method unusable for such flows. In such situations, in which use of the DSMC method is inefficient or not possible and continuum techniques are inaccurate, the use of a simplified form of the Boltzmann equation, such as the Bhatnagar–Gross–Krook (BGK) equation, can be considered. A method based on the solution of the BGK/ellipsoidal statistical BGK (ES-BGK) equation is expected to be more efficient than the DSMC method when applied to the low-Knudsen-number flows and more accurate than the solution of the Navier–Stokes (NS) equations for the high-Knudsen-number flows. For example, an application in which the BGK method could be accurately and efficiently used is in the modeling of the dense near-equilibrium flows in MEMS ($Kn \sim 0.01$, $Re \sim 1000$), in which the characteristic size of the device renders the use of continuum techniques questionable. Furthermore, because MEMS flows can be typically dense and subsonic, a particle may suffer several collisions per time step, causing the modeling of all these collisions to make the DSMC method expensive [12]. The work presented in this paper is a first step in the development of a hybrid approach wherein the DSMC and BGK methods will be suitably combined to minimize the computational time for multiscale simulations such as internal/external supersonic expansions to vacuum.

First we review the literature on past research related to solving the BGK and ES-BGK equations. Numerical solution of the BGK equation is obtained by either the deterministic (such as finite volume methods [12,13]) or the statistical methods. The comparative study of the two methods of solving the BGK equation was carried out in [14] by simulating supersonic expansions to vacuum in a nozzle, considering DSMC solution as the benchmark. It was shown that the statistical methods of solving the BGK equation are four times more

Received 12 June 2009; revision received 3 December 2009; accepted for publication 17 December 2009.

*Graduate Student, Department of Aerospace Engineering. Student Member AIAA.
†Postdoctoral Researcher, Department of Aerospace Engineering. Member AIAA.
‡Professor, Department of Aerospace Engineering. Associate Fellow AIAA.

numerically efficient than the deterministic finite volume BGK method and twice as efficient as the DSMC method. The statistical method of solving the BGK equation was first proposed by Nanbu [15] and extended by Gallis and Torczynski [12] to model the ES-BGK equation, which corrected for the unphysical value of the Prandtl number associated with the BGK equation. Andries et al. added rotational degrees of freedom to the statistical method [13] for solving a near-continuum diatomic flow of nitrogen over a ramp with a flap deflection of 25 deg.

A number of these authors studied flow over a flat plate. Gallis and Torczynski [12] used the BGK and ES-BGK methods to simulate compressible flow of argon gas over a flat plate with a Knudsen number of 0.025 (based on the length of the plate) and obtained good agreement with DSMC. Similarly, Andries et al. [13] studied compressible flow of a near continuum monoatomic gas over a flat plate where $Kn = 0.005$. They used a random particle numerical method [13] to solve the Boltzmann equation as well as the ES-BGK model. The ES-BGK solution was found to agree much more closely with the Boltzmann solution than the BGK method. Finally, Omar et al. [16] used a flux vector splitting BGK scheme to solve the Navier–Stokes equations to study laminar viscous flow problems. In their work, the freestream conditions for the study of laminar flow over a flat plate were a Mach number of $M_\infty = 0.2$, density of $\rho_\infty = 0.00283\ \mathrm{kg/m^3}$, and $T_\infty = 388.9$ K. In their flux vector splitting BGK scheme, the flux functions of the convective terms of the NS equations were approximated by the BGK scheme and the latter approach was found to agree well with the experimental data and the Roe flux difference splitting scheme.

In the present work, we consider a one-dimensional compressible semirarefied argon gas flow over a flat plate. The Knudsen number based on the boundary-layer thickness is of the order of 0.01. The problem is studied theoretically and numerically for two cases corresponding to adiabatic and isothermal wall conditions. The theoretical solution of the flow problem is obtained by NS equations following compressible boundary-layer theory [17]. Because the present work considers a semirarefied gas, the boundary-layer theoretical results were modified to include velocity slip and temperature jump corrections to the boundary conditions to account for flow rarefaction. The theoretical formulation is solved by the shooting technique (as described in Sec. II). The numerical techniques used in the present work include the DSMC method and the statistical solutions of the BGK and ES-BGK equations. We compare the solutions obtained by the statistical BGK and ES-BGK methods with those obtained from the theory and the benchmark DSMC method.

Such a comparison is performed to provide insight into the features of the statistical BGK/ES-BGK schemes and to the BGK method in general. Even though the method is not limited to simple gases [18], argon was used as the working gas so that the basic features of the method could be understood, avoiding the additional complication of translational–rotational relaxation. A large number of particles per cell was used to ensure that the influence of the number of particles per cell is eliminated for all three statistical methods. As will be shown in the discussion of results, the careful comparison captures a weak oblique shock wave appearing at the leading edge of the flat plate.

The outline of the remainder of the paper is as follows. In Sec. II, we briefly explain the theoretical method (along with the added velocity slip and temperature jump corrections to the boundary conditions) to obtain the flowfield solution for compressible gas flow over the flat plate. Section III is devoted to brief discussions about the different numerical methods used in the present work and their implementation. The results of the current work are presented and discussed in Sec. V. A comparison of the computational time and numerical parameters for the numerical methods is also presented. In Sec. VI, we present the conclusions.

II. Theoretical Solution of Compressible Boundary Layer over a Flat Plate with Slip

The theoretical solution of supersonic laminar flow over a flat plate is given by compressible boundary-layer theory. The theory assumes the gas to be calorically perfect, that is, with a constant specific heat capacity, whereas viscosity and thermal conductivity are considered to be temperature dependent. For the present case of compressible flow over a flat plate, a self-similar solution in the boundary layer may be obtained. In general, in the physical space (x, y), the velocity profiles at two different locations, x_1 and x_2 along the surface, are different, that is, $u(x_1, y) \neq u(x_2, y)$. However, under an appropriate independent variable transformation, it is possible to obtain flowfield profiles independent of the location along the surface of the flat plate. Thus, in the transformed plane (ξ, η), the velocity profile becomes independent of ξ and is given by $u = u(\eta)$. Boundary layers that exhibit such a property are called self-similar boundary layers, and the solutions for such boundary layers are termed self-similar solutions [17].

The governing equations in the transformed plane, (ξ, η), are derived from those in the physical space, (x, y) [17], and are given as follows:

$$(Cf'')' + ff'' = 0 \tag{1}$$

$$\left(\frac{C}{Pr}g'\right)' + C\frac{u_e^2}{h_e}\left(f''\right)^2 = 0 \tag{2}$$

In Eqs. (1) and (2), $C = \rho\mu/\rho_e\mu_e$, where ρ and μ are the density and dynamic viscosity, respectively, and the subscript e represents their freestream values. $Pr = \mu c_p/\kappa$ is the Prandtl number, where c_p is the specific heat capacity of argon at constant pressure and κ is the thermal conductivity of argon. It should be noted that Eqs. (1) and (2) are ordinary differential equations in terms of the single independent variable η, and the usual assumption that pressure is constant and equal to the value at the edge of the boundary layer is used.

The solutions to these equations using the appropriate boundary conditions provide variations of velocity and enthalpy across the boundary layer. To obtain the solution, the independent variables in transformed space (ξ, η) are related to those in the physical space (x, y) by the following transformation:

$$\xi = \int_0^x \rho_e u_e \mu_e \,\mathrm{d}x \tag{3}$$

$$\eta = \frac{u_e}{\sqrt{2\xi}}\int_0^v \rho \,\mathrm{d}y \tag{4}$$

where ρ_e, u_e, and μ_e represent the freestream values of density, velocity, and dynamic viscosity, respectively. The dependent variables of Eqs. (1) and (2) can be written in terms of the transformed variables as

$$\frac{u}{u_e} = \frac{\partial f}{\partial \eta} = f' \tag{5}$$

$$g = \frac{h}{h_e} \tag{6}$$

where h_e represents the freestream value of enthalpy. The solution of the boundary-layer equations given by Eqs. (1) and (2) also requires five boundary conditions at the wall ($\eta = 0$). Three of these boundary conditions for no-slip flow at the wall are

$$f(0) = f'(0) = 0, \qquad g(0) = g_w \text{ for an isothermal wall}$$
$$g'(0) = 0 \text{ for an adiabatic wall} \tag{7}$$

However, in our present problem the Knudsen number is $\sim$0.01, based on the boundary-layer thickness, thereby causing a velocity slip and temperature jump at the wall. The magnitudes of the velocity slip and the temperature jump are given by Maxwell and Smoluchowski in Liou and Fang [4], and reexpressed here in the transformed plane as

$$f'(0) = \frac{1}{u_e}\frac{2-\sigma_v}{\sigma_v}\lambda\frac{\partial u}{\partial y} \tag{8}$$

$$g(0) = \frac{T_w}{T_e} + \frac{1}{T_e}\frac{2-\sigma_T}{\sigma_T}\frac{2\gamma}{\gamma+1}\frac{\lambda}{Pr}\frac{\partial T}{\partial y} \tag{9}$$

where σ_v and σ_T are the tangential momentum and thermal accommodation coefficients, λ is the mean free path of the gas, $\frac{\partial u}{\partial y}$ is the velocity gradient normal to the wall, γ is the specific heat ratio of the gas, and T_w is the plate temperature. Therefore, the boundary conditions at the wall ($\eta = 0$) for a finite Knudsen number flow are

$$f(0) = f'(0) \neq 0; \qquad g(0) \neq g_w, \text{ isothermal wall}$$
$$g'(0) = 0, \text{ adiabatic wall} \tag{10}$$

The values of velocity and temperature gradients (normal to the wall) in Eqs. (8) and (9) are obtained from the DSMC solutions. Because $f''(0)$ and $g'(0)$ (for the isothermal wall) or $f''(0)$ and $g(0)$ (for the adiabatic wall) are not known a priori, we solve the ordinary differential equations given by Eqs. (1) and (2), numerically with the shooting technique [17]. In the shooting technique, approximate values of $f''(0)$ and $g'(0)$ (for the isothermal wall) or $f''(0)$ and $g(0)$ (for the adiabatic wall) are assumed, and Eqs. (1) and (2) are numerically integrated across the boundary layer up to a large value of η such that $f'(\eta)$ and $g(\eta)$ become relatively constant with η, corresponding to the freestream conditions. If the resulting values of $f'(\eta)$ and $g(\eta)$ at large η approach a value of unity, then the assumption is understood to be correct; otherwise, different values are chosen for $f''(0)$, and $g'(0)$ or $g(0)$ and the procedure is repeated until we obtain unity values for $f'(\eta)$ and $g(\eta)$ at the edge of the boundary layer. Good starting assumptions for $f''(0)$ and $g'(0)$ are values on the order of 0.4 to 1.0. In the case of an adiabatic wall, the value of $g(0)$ is needed instead of $g'(0)$ and can be obtained from the following equation for a compressible flow [17]:

$$g(0) = 1 + r\frac{u_e^2}{2h_e} \tag{11}$$

where r is the recovery factor and is equal to $Pr^{1/2}$ for a laminar flow.

Surface quantities related to the skin friction and heat transfer coefficients may also be obtained from boundary-layer theory. The shear stress is defined as

$$\tau_w = \left[\mu\frac{\partial u}{\partial y}\right]_w \tag{12}$$

where μ is the dynamic viscosity of the fluid near the wall and is related to freestream dynamic viscosity, μ_e, as

$$\frac{\mu}{\mu_e} = \left(\frac{T}{T_e}\right)^n \tag{13}$$

where n is the viscosity temperature dependence coefficient equal to 0.81 for argon. The corresponding local skin friction coefficient, C_f, and the heat flux to the wall, q_w, are given by

$$C_f = \frac{\tau_w}{\frac{1}{2}\rho_e u_e^2} = \frac{[\mu\frac{\partial u}{\partial y}]_w}{\frac{1}{2}\rho_e u_e^2} \tag{14}$$

$$q_w = \left[\lambda\frac{\partial T}{\partial y}\right]_w \tag{15}$$

where λ is the thermal conductivity of the fluid near the wall. It may be obtained from the dynamic viscosity using the usual kinetic relationship:

$$\lambda = (15k/4m)\mu,$$

where k is the Boltzmann constant and m is the mass of a particle of the gas. Finally, the local heat transfer coefficient is defined by the Stanton number, C_h, and is given by

$$C_h = \frac{q_w}{\rho_e u_e c_p(T_{\text{aw}} - T_w)} = \frac{[\lambda\frac{\partial T}{\partial y}]_w}{\rho_e u_e c_p(T_{\text{aw}} - T_w)} \tag{16}$$

where c_p is the specific heat capacity of the fluid and T_{aw} is the adiabatic wall temperature, which is related to the total temperature, T_0, as

$$\frac{T_{\text{aw}} - T_e}{T_0 - T_e} = Pr^{1/2} \tag{17}$$

The flow and surface quantities thus obtained from the boundary-layer equations will be used for comparison with the statistical methods in Sec. V.

III. Computational Methods

The computational methods used in the present work approximate the Boltzmann equation [19], which is one of the most basic equations of kinetic theory:

$$\frac{\partial}{\partial t}(nf) + v\cdot\frac{\partial}{\partial \mathbf{r}}(nf) + \mathbf{F}\cdot\frac{\partial}{\partial \mathbf{v}} = \int_{-\infty}^{\infty}\int_0^{4\pi} n^2(f^*f_1^* - ff_1)v_r\sigma\,\mathrm{d}\Omega\,\mathrm{d}\mathbf{v} \tag{18}$$

where f and f_1 are the precollision distribution functions of the two colliding particles and f^* and f_1^* are the postcollision distribution functions, $\mathbf{F}$ is an external force applied to the particles (assumed to be zero for the present study), σ is the cross section of the binary collision and Ω is the solid angle, v_r is the relative velocity of the colliding particles, and n is the number density. Next, we briefly present the major features of the DSMC and BGK/ES-BGK methods and their implementation.

A. Direct Simulation Monte Carlo Method

The DSMC method [19] is a discrete particle simulation method that uses probabilistic (Monte Carlo) simulation to solve the Boltzmann equation for finite-Knudsen-number fluid flows. It is a technique for the computer modeling of a gas flow by simulated particles, each one representing a large number of real atoms/molecules. The velocity components and position coordinates of these particles are updated by modeling their motions and collisions, which in turn are uncoupled. The uncoupling of motions and collisions restricts the time step to be on the order of (usually smaller than) the mean collision time. The cell size is kept on the order of the mean free path or less.

A detailed description of the DSMC method can be found in [19], so that here we provide only the specific details pertinent to the present work. We have used the statistical modeling in a low density environment (SMILE) computational solver to obtain the DSMC solution. Details of the solver may be found in [20]. The important features that are used in the present work include different grids for collisions and macroparameters, both of which are two-level adaptable Cartesian grids, and the parallel implementation with efficient load balancing techniques. The majorant frequency scheme is used for selecting pairs of colliding particles [21]. The variable hard sphere (VHS) model is used for modeling the particle interactions. Diffuse reflection with full/no thermal accommodation is assumed on the plate for different cases. Solutions independent of grid, time step, and number of particles are obtained.

B. Statistical Method for Solution of the Bhatnagar–Gross–Krook and Ellipsoidal Statistical Bhatnagar–Gross–Krook Model Kinetic Equations

The statistical BGK methods are implemented in the DSMC code, SMILE [20]. The major difference from the DSMC method is in the modeling of the collisional relaxation term. In the statistical BGK methods, a fraction of particles are randomly selected in each computational cell, per time step, based on the local collisional frequency. They are then assigned new velocities from either a local

Maxwellian or an ellipsoidal distribution function for the BGK or the ES-BGK methods, respectively. DSMC, in contrast to the BGK methods, models the collisional relaxation through individual collisions of particles. It is this key difference in the DSMC and BGK approaches that suggests that the latter will be more efficient at high flow densities for which the collision rate is sufficiently high that it is not necessary to model individual collisions.

The relaxation rate at which the flow relaxes toward equilibrium in the statistical BGK method is governed by the characteristic relaxation frequency given by

$$\nu = Pr \cdot nk\left(\frac{T_{\text{ref}}^{\omega}}{\mu_{\text{ref}}}\right)T^{1-\omega} \tag{19}$$

where Pr is the Prandtl number (assumed to be unity for the BGK equation), k is the Boltzmann constant, T is the local translational temperature in a cell, and μ_{ref} is the gas dynamic viscosity at T_{ref}.

In the collisional relaxation procedure, the number of particles selected (N_c) in each cell for velocity sampling from the local Maxwellian distribution depends on the relaxation frequency and the time step as

$$N_c = \text{int}(N(1 - \exp(-\nu\Delta t)) \tag{20}$$

where Δt is the time step, N is the number of particles in a cell, and int is an operator that returns the nearest smaller integer. To compensate for the systematic error that such an operator produces, one more particle is added to the list of preselected particles with the probability

$$P_c = N(1 - \exp(-\nu\Delta t) - \text{int}(N(1 - \exp(-\nu\Delta t)) \tag{21}$$

The particles, which have been selected for velocity sampling, are assigned new thermal velocities from a Maxwellian distribution at the local cell based temperature by

$$v_x^1 = \cos(2\pi R_1)\sqrt{-\ell_n(R_2)} \cdot \sqrt{2kT/m} \tag{22}$$

$$v_y^1 = \sin(2\pi R_1)\sqrt{-\ell_n(R_2)} \cdot \sqrt{2kT/m} \tag{23}$$

$$v_z^1 = \cos(2\pi R_3)\sqrt{-\ell_n(R_4)} \cdot \sqrt{2kT/m} \tag{24}$$

where R_1 through R_4 are random numbers uniformly distributed between 0 and 1, and the superscript 1 indicates the velocity after the assignment of new thermal velocities. The velocities of particles that have not been preselected remain unchanged.

Proposed by Holway [22] and Cercignani [23] as a modification to the BGK equation, the ES-BGK method corrects for the unphysical value of the unity Prandtl number in the BGK method. The correction assumes special significance, when the flow conditions are such that the thermal conductivity is important, as will be discussed in Sec. V. The equilibrium distribution function in the ES-BGK model is the local anisotropic three-dimensional Gaussian, f_G, referred to as the ES distribution, and the collision term is approximated as

$$\left[\frac{\partial}{\partial t}(nf)\right]_{\text{collision}} = \nu n(f_G - f) \tag{25}$$

The characteristic relaxation frequency with the physically correct Prandtl number is calculated using Eq. (19). The procedure for selecting particles for which the velocities are reassigned is the same as for the BGK method discussed earlier. The selected particles are assigned velocities from a local Maxwellian distribution function, as in BGK, but then their velocity components are modified to conform to the ES distribution:

$$v_i^2 = S_{ij} \cdot v_j^1 \tag{26}$$

where $\mathbf{v}^2$ designates the modified velocity components and S_{ij} is given by

$$S_{ij} = \delta_{ij} - \frac{1 - Pr}{2Pr}\left[\frac{1}{kT}\frac{N}{N-1}(\langle mv_iv_j\rangle_a - \langle mv_i\rangle_a\langle mv_j\rangle_a/\langle m\rangle_a) - \delta_{ij}\right] \tag{27}$$

where the symbol $\langle\ \rangle_a$ represents an averaging over all the particles in a cell, δ_{ij} is the Kronecker delta function, m is the mass of a particle, and the indices i, j refer to the three Cartesian components of velocity.

IV. Numerical Parameters

For all statistical methods such as BGK or DSMC several numerical aspects should be taken into account to ensure that the solution is independent of the choice of numerical parameters of the method. For example, the size of the computational domain should be such that it accommodates all of the flow features that are relevant to the problem, but at the same time is not larger than necessary because this may adversely affect the computational time. If there are strong gradients in the flow, the final mesh resolution must be adequate to resolve them. In our particular case, we paid close attention to the mesh resolution in the regions of the flow close to an oblique shock wave at the plate leading edge (to be discussed further in Sec. V) and in the region close to the plate. In addition, there must be a sufficient number of particles per cell to ensure a sufficient number of collisions per time step, in the case of DSMC, or to achieve relaxation in the BGK approaches.

To that end, a number of computational parameters were chosen to ensure numerical convergence, with Table 1 summarizing the key numerical parameters used for the three different statistical methods for both thermal boundary conditions. The length and width of the computational domain were varied, and then the final values of the computational domain were selected in such a way such that the further increase in its size did not alter the solution. This resulted in a computational domain for all cases of 0.1×0.015 m, where 0.1 m is the length of the flat plate and 0.01 m is the distance normal to the flat plate. The cell size used in the numerical computations is less than the mean free path. Likewise the time step is such that a molecule does not cross more than one cell per time step, or the time step is less than the mean time between collisions. The final values of the collision cell size and time step are 5×10^{-5} and 4×10^{-8}, respectively. Because one of our goals is to compare the solutions among three different statistical approaches, we need to ensure that the influence of the number of particles per cell is eliminated in all methods. For that reason, a larger than required number of particles per cell, ~100, was used to perform the simulations shown in Sec. V. Sampling occurred over 100,000 time steps for all three methods.

The computational procedure used to implement the BGK and ES-BGK approaches has been provided in [24]. The salient points are summarized here as follows. We start the simulation by disabling the collisional relaxation step in the BGK calculation to simulate only the convection of molecules in a free molecular manner for a predefined number of time steps (usually 1000). This has the effect of initializing the flowfield so that the collision frequency may be computed. Having initialized the flowfield, we proceed with the BGK solution, turning on the collisional relaxation procedure in the code. The collisional procedure is continued in each cell until the overall number of particles in the computational domain remains constant, which requires about 80,000 time steps. After that, we sample the quantities necessary to compute the flow properties,

Table 1 Comparison of numerical parameters used in the three simulation approaches (where the computational domain for all cases is 100 × 15 mm)

Parameters	DSMC	BGK	ES-BGK
Number of particles (10^6)	20	80	80
Number of cells (10^6)	0.8	0.8	0.8
Time step (10^{-8} s)	2.5	2.5	2.5

which requires about 100,000 time steps, at a time step of 4×10^{-8} s. Note that this procedure is used for both the statistical BGK and ES-BGK implementations.

V. Results and Discussion

A laminar gas flow of argon over a flat plate of zero thickness is studied at a Reynolds number of 3746, based on the length of the plate (0.1 m). The freestream conditions correspond to a Mach number of 3 and an ambient temperature and pressure of 273 K and 48.88 N/m^2, respectively. Flow solutions and surface quantities are presented for three numerical methods, BGK, ES-BGK, and DSMC, and the boundary-layer theory with slip correction. The two thermal boundary conditions of an adiabatic and isothermal plate wall are considered. The working gas, argon, has a reference dynamic viscosity of $\mu_{\text{ref}} = 2.117 \times 10^{-5}$ Pa at a reference temperature of 273 K, a viscosity temperature index of $n = 0.81$ used in the VHS model [Eq. (13)], and an atomic diameter of 4.17×10^{-10} m. The Knudsen number based on the boundary-layer thickness is of the order of 0.01.

A. Flow over the Adiabatic Flat Plate

The flat plate is assumed to be insulated; thus, there is no heat transfer to or from the flat plate, that is, $g'(0) = 0$ and a diffuse reflection with $\sigma_v = 1$ is used in Eq. (8). To solve for $g(0)$ in Eq. (11), a value of $r = Pr^{1/2}$ and the postshock freestream conditions are used. The variation of Knudsen number, based on the boundary-layer thickness, along the length of the plate is shown in Fig. 1. The abscissa in Fig. 1 and in subsequent figures is normalized by the length of the plate, $L = 0.1$ m, and x is the distance from the flat plate leading edge. It can be seen that the Knudsen number is of the order of 0.01, thereby resulting in a finite velocity slip and temperature jump on the surface of the plate. The top portion of Fig. 2 shows the Mach number contours predicted by the ES-BGK method, where, again, the abscissa and ordinates are normalized by the length of the plate, L. The figure shows that the flow is supersonic with a shock wave appearing at the leading edge of the plate. We can compare the shock wave angle at the leading edge predicted by oblique shock wave theory [25] with that predicted by the simulations. Figure 3 shows the location of the edge of the boundary layer, or, in other words, boundary-layer growth obtained by the ES-BGK method, along the length of the adiabatic flat plate. Boundary-layer growth profiles obtained by the DSMC and BGK methods agree very well with the ES-BGK method with a maximum difference of less than 1.5%. If we assume that the shock deflection angle (see Fig. 4.6 of [25]) can be approximated by a wedge of angle corresponding to the initial slope of the adiabatic flat plate boundary-layer curve shown in Fig. 3, we

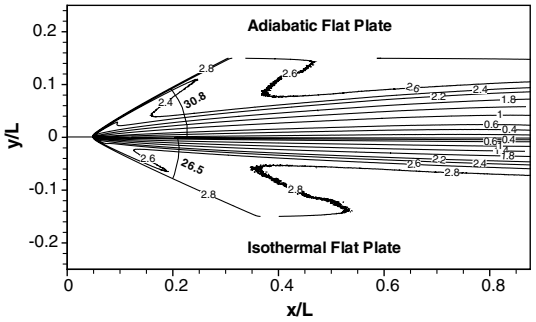

Fig. 2 Mach number contours showing the shock wave angle formed due to the formation of boundary layers in supersonic flow over an adiabatic flat plate (top) and an isothermal flat plate (bottom).

obtain a deflection angle of 13.65 deg. From oblique shock wave theory for a freestream Mach number of 3, this deflection angle gives a shock angle of 30.5 deg. It can be observed from Fig. 2 that the shock angle is ~30.8 deg, which is quite close to the value of 30.5 deg predicted by the oblique shock theory. Next we show that the boundary layer formed over the adiabatic flat plate in the ES-BGK simulation is self-similar, that is, the boundary-layer profile remains independent of the location along the length of the flat plate. In all the subsequent figures for flow over the adiabatic flat plate, the velocity and temperature are normalized by their values at the edge of the boundary layer, u_e and T_e, respectively. Because of the presence of the weak oblique shock at the leading edge, these values, even at $x/L = 0.75$, are slightly different from the preshock freestream conditions, as shown in Table 2. Therefore, the values indicated as postshock adiabatic boundary conditions are used to normalize the velocity and temperature profiles, rather than the respective preshock values. The ordinate is normalized by the quantity $x/\sqrt{Re_x}$ and is referred to as y^* in the figures. Figure 4 shows the velocity and temperature profiles obtained by the ES-BGK method at the two stations along the surface of the flat plate at $x/L = 0.5$ and 0.75. It can be seen from the figure that the velocity and temperature profiles at the two stations are quite close to each other, demonstrating, as expected, that the boundary-layer solutions are essentially self-similar. The DSMC and BGK methods also show self-similar velocity and temperature profiles, with a maximum difference of less than 1% between the velocity and temperature profiles at the two stations.

Having demonstrated that the numerical solutions of the boundary-layer flow are self-similar, we compare the solutions with compressible boundary-layer theory. Because the theory does not take into account the presence of a shock wave, we choose a location

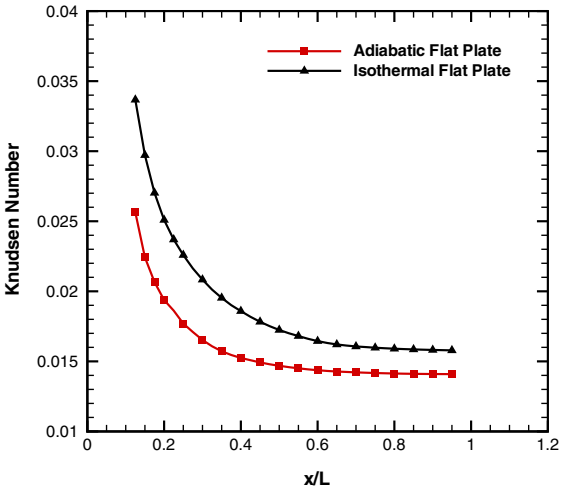

Fig. 1 Variation of the Knudsen number based on boundary-layer thickness along the length of the plate for the adiabatic and isothermal wall boundary conditions.

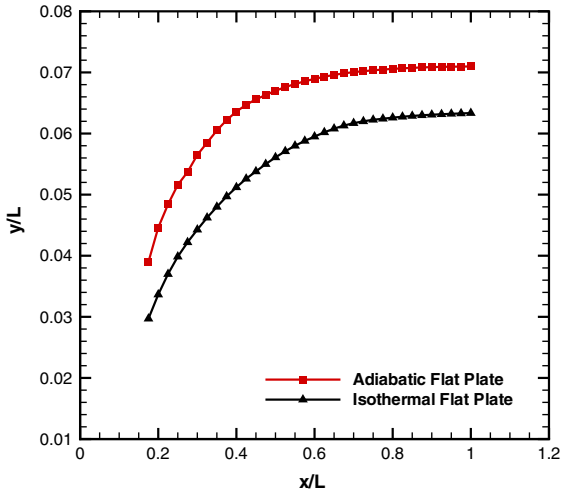

Fig. 3 Location of the boundary-layer edge for flow over the adiabatic and isothermal flat plates obtained by the ES-BGK method.

Table 2 Postshock freestream conditions at $x/L = 0.75$ used for calculating theoretical boundary-layer flow

Location	Velocity, u_e, m/s	Temperature, T_e, K	Density, kg/m^3
Preshock	923.4	273	0.00086
Postshock, adiabatic boundary condition	899.5	315.5	0.00101
Postshock, isothermal boundary condition	910.5	291.0	0.00095

sufficiently far from the leading edge to compare with the numerical results and also use the corrected boundary-layer edge conditions, u_e and T_e, given in Table 2 for the respective normalizations, as mentioned earlier. Figure 5 shows a comparison of velocity and temperature profiles obtained from the numerical methods and boundary-layer theory. The theoretical value of the velocity slip as given by Eq. (8) was used to generate the theoretical solution of the flowfield as described in Sec. II. It is evident from Fig. 5a that the velocity profiles produced by the numerical methods agree well with the theoretical solution. The maximum departure from the theoretical profile is shown by the statistical BGK method, although it is less than 5%. Close examination of the figure also shows that there exists a velocity slip at the wall and that the magnitude of the velocity slip can be estimated by Eq. (8) using the velocity gradient at the wall from the DSMC solution. Using this procedure, the boundary-layer theory predicted slip ranges from 30 to 33 m/s compared to the values obtained directly from the numerical methods of 40–42 m/s. Considering that the estimation of gradients from a statistical method has a statistical error and that the boundary-layer theory assumes the first-order Maxwell–Smoluchowski relationship for velocity slip [4], which is strictly applicable only for an isothermal wall, the agreement between the theory and modeling and simulation is good.

Figure 5b compares the temperature profiles obtained by the numerical methods with boundary-layer theory. Because the adiabatic boundary condition is imposed on the surface, the heat transfer to or from the flat plate, effectively proportional to $\partial T/\partial y$, at the surface is zero, resulting in a temperature profile normal to the wall. In addition, from the outer edge of the boundary layer to the wall, the kinetic energy decreases to almost zero (accounting for a finite velocity slip) or, equivalently, is transformed to thermal energy. This transformation of kinetic to thermal energy causes the gas temperature to monotonically increase toward the wall, as shown in the Fig. 5. Also, it can be seen that the temperature profiles produced by the DSMC and statistical ES-BGK methods agree quite well with the theoretical solution. The temperature profile for the BGK method, however, differs because the BGK approximation corresponds to an incorrect Prandtl number of unity for the gas. This incorrect simplifying assumption results in incorrect transport properties such as thermal conductivity, which in turn affect the temperature profile. However, it can be shown that the solution produced by the BGK method is consistent with the theory of compressible flow for a gas of unity Prandtl number as follows. The temperature at the surface of the flat

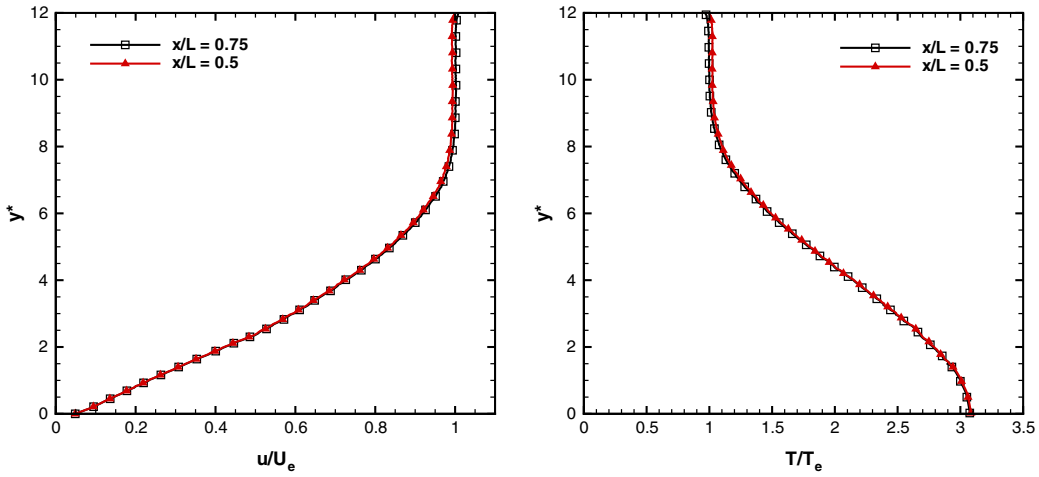

Fig. 4 Comparison of profiles at two stations ($x/L = 0.5$ and $x/L = 0.75$) obtained by the ES-BGK method for flow over the adiabatic flat plate: a) velocity, and b) temperature.

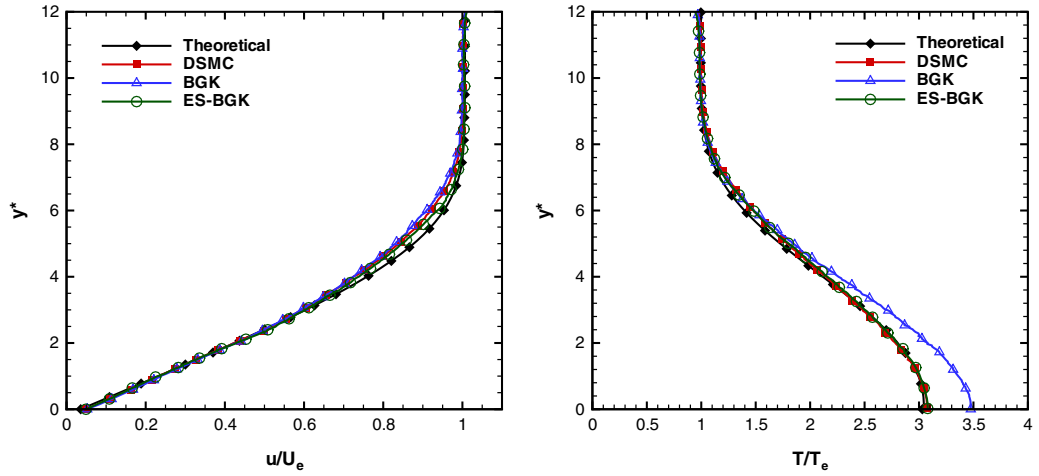

Fig. 5 Comparison of profiles obtained by numerical methods with those obtained by theoretical method for flow over the adiabatic flat plate at $x/L = 0.75$: a) velocity, and b) temperature.

plate for an adiabatic compressible flow of a gas with unity Prandtl number (translating into a recovery factor of unity) is given as [25]

$$\frac{T_w}{T_e} = 1 + \frac{\gamma - 1}{2} M^2 \tag{28}$$

Using the freestream conditions at $x/L = 0.75$ as given in Table 2, Eq. (28) gives a nondimensionalized temperature of 3.47 at the wall, which is very close to the value of 3.46 predicted by the statistical BGK method, as can be seen in Fig. 5b.

Using the velocity gradients derived from the simulations, we now compare the coefficient of skin friction and Stanton number (as defined in Sec. II) along the length of the plate. For an adiabatic plate, there is no heat transfer to or from the plate; therefore, only the skin friction coefficient is discussed. Also, because compressible boundary-layer theory is not valid in the proximity of the leading edge of the plate [17], we compare skin friction data downstream of $x/L = 0.25$. Figure 6 shows a comparison of the skin friction coefficient obtained by the ES-BGK solution, the better of the two BGK methods, with the theoretical solution. It can be seen that the two agree fairly well, with a maximum difference of about 4%. The slight shift in the two results is due to the small differences in the velocity gradients, as shown in Fig. 5a.

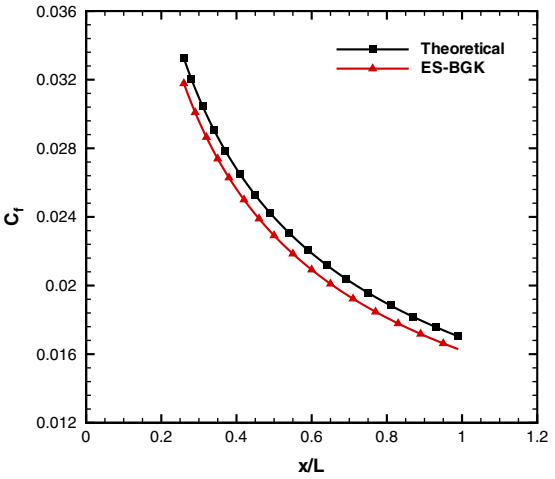

Fig. 6 Comparison of coefficient of friction obtained by statistical ES-BGK method with that obtained by theoretical method for flow over the adiabatic flat plate.

B. Flow over the Isothermal Flat Plate

The flat plate is modeled assuming a uniform, constant temperature of 273 K with diffuse reflection ($\sigma_v = 1$) and full thermal accommodation ($\sigma_T = 1$). Figure 1 shows the variation of Knudsen number, based on the boundary-layer thickness, obtained by the ES-BGK method along the length of the isothermal plate. The boundary-layer growth, obtained by the ES-BGK method, in turn is shown in Fig. 3. The Knudsen numbers are similar to those for the adiabatic plate, but are slightly higher because, as Fig. 3 shows, the boundary-layer thickness is smaller for the isothermal flat plate. The DSMC and BGK methods agree well with the ES-BGK method in terms of boundary-layer growth with a maximum difference of less than 1.5%. Again, the Knudsen number is in the range in which there is a finite velocity slip and temperature jump at the surface of the plate. An examination of the Mach number contours in the bottom portion of Fig. 2 shows that similar to the adiabatic case an oblique shock wave is formed at the leading edge of the plate. We can compare the shock wave angle with that given by the oblique shock wave relationships [25]. In a manner similar to the adiabatic boundary condition case, we can obtain a flow deflection angle formed by the boundary layer of 9.95 deg, a deflection angle smaller compared to the value of 13.65 deg for flow over the adiabatic flat plate. A comparison of the top and bottom portions of Fig. 2 shows that the boundary-layer growth is greater over the adiabatic plate because, for the cold, isothermal wall at 273 K, the flow density in the boundary layer is much higher than that in the case of adiabatic flat plate. Because the density is higher, the same mass flow rate exiting the boundary layer can be achieved with a boundary layer of a smaller thickness. Therefore, the cold isothermal wall results in a thinner boundary layer and, hence, a smaller deflection angle. The shock angle given by oblique shock wave theory for a deflection angle of 9.95 deg and freestream Mach number of 3 is 27.33 deg. It can be seen from Fig. 2 that the shock wave angle obtained from the simulations is ~26.5 deg, which agrees well with the value of 27.33 deg predicted by the oblique shock theory.

Next we show that the boundary layer formed by flow over the isothermal flat plate is self-similar. As before, Fig. 7a shows the normalized velocity and Fig. 7b the temperature profiles obtained by the ES-BGK method as a function of the normalized distance through the boundary layer, y^*. Again the comparison is presented at the two stations, $x/L = 0.5$ and 0.75, using the values at the boundary-layer edge slightly modified by the presence of the shock at the leading edge, given in the last row of Table 2. It can be seen that the velocity and temperature profiles are essentially self-similar in the transformed coordinate. Similar profiles obtained by the DSMC and the BGK methods also show self-similarity, with a maximum difference of less than 1% between the velocity and temperature profiles at the two stations.

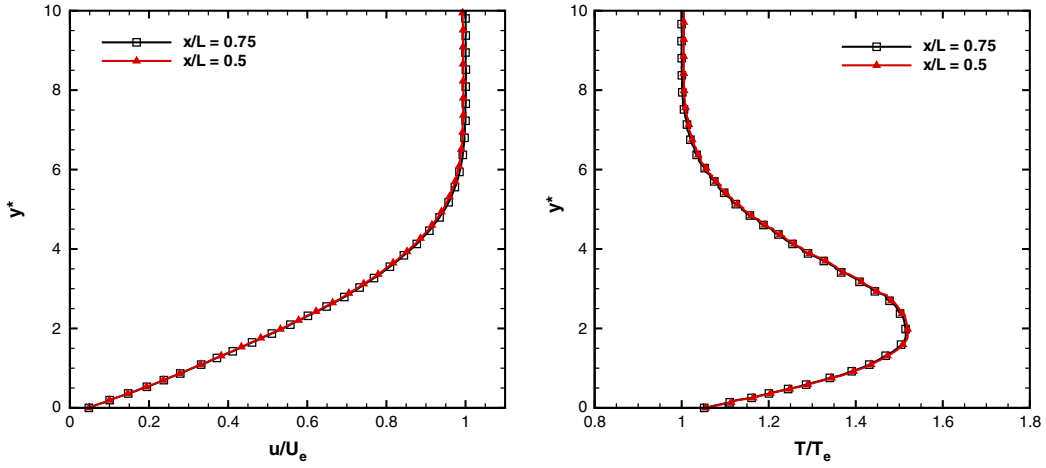

Fig. 7 Comparison of profiles at two stations ($x/L = 0.5$ and $x/L = 0.75$) obtained by the ES-BGK method for flow over the isothermal flat plate: a) velocity, and b) temperature.

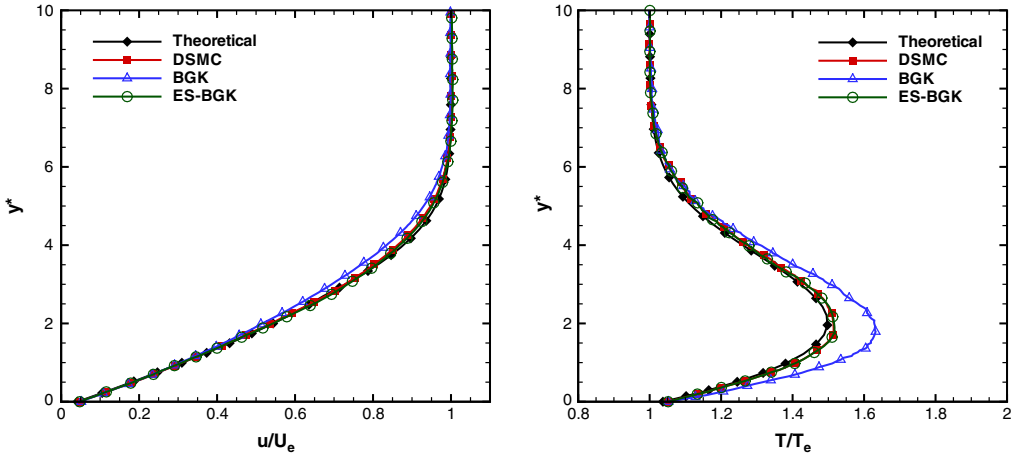

Fig. 8 Comparison of profiles obtained by the numerical methods with the theoretical boundary flow equations for the isothermal flat plate: a) velocity, and b) temperature.

To compare the numerically simulated flowfield velocity and temperature profiles with the theoretical boundary-layer solution for the isothermal flat plate, we choose a position sufficiently far from the oblique shock wave using the corrected boundary-layer edge conditions given in Table 2 at $x/L = 0.75$. Figure 8a compares the velocity profiles obtained using the numerical methods with boundary-layer theory. It can be seen in Fig. 8 that there is velocity slip at the flat plate and, again, its magnitude can be estimated with Eq. (8) using the velocity gradient value from the DSMC solution. The theoretical value of the velocity slip was found to be 36–39 m/s as compared to a value of 40–42 m/s produced by all the statistical numerical methods. Again, within the statistical error, the agreement between theory and simulation is good. The boundary-layer theory value for the velocity slip is used to generate the entire theoretical velocity profile across the boundary layer. It is evident from Fig. 8 that the velocity profiles produced by the numerical methods agree well with the theoretical solution. The maximum departure from the theoretical profile is shown by the statistical BGK method, although it is less than 5%. It is worth noting that the velocity profile for flow over the isothermal flat plate is qualitatively similar to that over the adiabatic flat plate (as shown in Fig. 5). This similarity is because the specific thermal boundary condition does not directly impact the velocity profile, although it indirectly effects the boundary-layer thickness, as discussed earlier.

Figure 8b compares the temperature profiles obtained by the numerical methods with boundary-layer theory. It can be seen that, starting from the wall and going toward the outer edge of the boundary layer, the temperature first increases from its value at the wall, reaches a peak somewhere within the boundary layer, and then decreases to the value of temperature at the leading edge, T_e, at $x/L = 0.75$. It can also be seen that there is a temperature jump at the flat plate surface and its magnitude can be estimated by Eq. (9) using the temperature gradient value from the DSMC solution. The theoretical value of the temperature jump was found to be 27–30 K, as compared to 30–33 K predicted by the numerical methods, and the theoretical value of the temperature jump is used to generate theoretical solution of the flowfield. The temperature profiles predicted by the DSMC and ES-BGK methods, as shown in Fig. 8b, agree well with the theoretical solution with a maximum difference of less than 2% at the maxima of the temperature profile. The statistical BGK method produces a qualitatively similar profile, but it again differs from theory by a value of 7% because of the incorrect Prandtl number that affects the transport properties of the gas.

It is interesting to note that the temperature profiles for the two cases of flow over the adiabatic and isothermal plates are qualitatively different as can be seen by comparison of Figs. 5b and 8b. In the case of the adiabatic flat plate, the heat transfer to the plate, which is proportional to $\partial T/\partial y$, is forced to be zero, thereby making the temperature profile normal to the flat plate as was discussed earlier. For the case of flow over a cold, isothermal flat plate, the temperature close to the surface of the flat plate is forced to match the constant cold wall temperature (with some finite temperature jump). In this flow, the kinetic energy is also transformed to thermal energy in going from the outer edge of the boundary layer to the wall in a similar manner as for the flow over the adiabatic plate. However, for the isothermal case, the two effects of energy conversion and temperature slip combine to create a temperature profile with a parabolic shape in the boundary layer, as shown in Fig. 8b.

Finally, we compare the coefficient of skin friction, the Stanton number, and the ratio of skin friction to the Stanton number computed at the wall along the length of the plate, as defined in Sec. II. Similar to the adiabatic flat plate, we compare here the shear

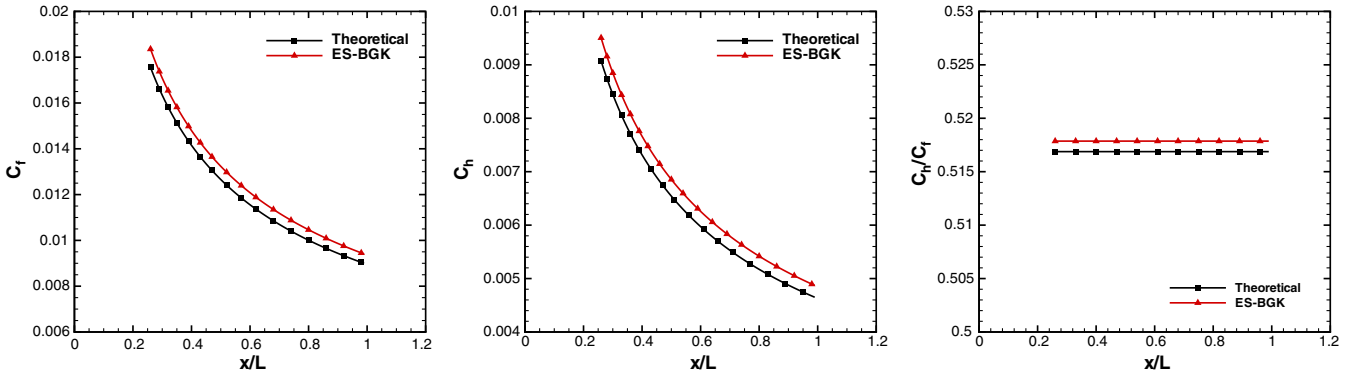

Fig. 9 Comparison obtained with the ES-BGK method and boundary-layer theory for flow over an isothermal flat plate: a) coefficient of friction, b) Stanton number, and c) ratio of Stanton number to skin friction coefficient.

Table 3 Comparison of numerical performance of the simulation approaches (both thermal boundary condition cases provide the same numerical performance)

Parameters	DSMC	BGK	ES-BGK
Time, CPUH	560	300	300
Number of particles, 10^6	9	5.0	5.0
Number of cells, 10^6	0.6	0.15	0.15
Time step, 10^{-8} s	4	8	8

stress and heat flux obtained by the ES-BGK solution with boundary-layer theory. It can be seen in Fig. 9 that the ES-BGK solution agrees fairly well with the theoretical solution, with a maximum difference of less than 4%. If we compare the coefficient of skin friction obtained in the present case of the isothermal plate with the earlier case of the adiabatic flat plate, we can see that skin friction coefficient is comparatively much higher in the latter case. This occurs because there are two factors that affect the skin friction coefficients: the velocity gradient and the dynamic viscosity [Eq. (14)]. Even though the velocity gradient is larger in the isothermal flat plate case, the dynamic viscosity of the fluid close to the wall is much larger for the adiabatic flat plate case. Of the two terms, the dynamic viscosity has the dominant effect on the skin friction coefficient. A comparison of the nondimensionalized heat flux, as given by the Stanton number, between the ES-BGK and boundary-layer theory is shown in Fig. 9. Good agreement is achieved between the two solutions with a maximum difference of less than 4%. Also, the ratio of the Stanton number and skin friction coefficient is plotted for the ES-BGK solution and boundary-layer theory. The agreement is remarkably good, with a maximum difference of about 0.2%. Furthermore, it is worth noting that the theoretical and the numerical value of the ratio of the Stanton number to the skin friction coefficient, C_h/C_f, is about 0.52 for the present problem of compressible laminar flow of argon, whereas the ratio would be 0.655 for the incompressible flow of argon as per incompressible boundary-layer theory [17].

C. Computational Efficiency

With the numerical accuracy of the BGK and ES-BGK methods in modeling well-known laminar boundary-layer flows established, we discuss the numerical efficiency of these methods as compared to DSMC method. To provide a consistent comparison, all three numerical approaches were used again to model flow over an isothermal plate with a cell size of 50 μm, a time step of 5×10^{-8} s, and approximately 100 particles per cell. A series of calculations with different numerical parameter sets was performed with the BGK and ES-BGK methods wherein cell size, time step, and number of particles per cell were varied to ensure that the solutions obtained with the aforementioned numerical parameters provided a numerically converged solution for these methods. The conclusions based on these sensitivity studies are equally applicable to the earlier case of flow over an adiabatic plate.

Table 3 compares the computational time required to reach a mesh converged solution for the three computational methods. The sensitivity study was carried out with an equal number of Intel 3 GHz Xeon processors. The comparison of computational times shows that the statistical BGK and ES-BGK methods are almost two times more efficient than the DSMC method. The average number of required particles per cell is found to be about 32 for statistical BGK/ES-BGK methods, whereas for the DSMC method it is about 15. It can also be inferred that the cell size could be made larger in the statistical BGK and ES-BGK methods, as compared to the DSMC calculation, which would enable these BGK methods to be used for higher-pressure cases, in which DSMC cannot be used due to the high computational cost.

VI. Conclusions

Compressible flow over a flat plate was studied at a Knudsen number of $\sim$0.01 based on the boundary-layer thickness, a Mach number of 3, and a Reynolds number of 3746. Two thermal boundary conditions were considered: an adiabatic and isothermal flat plate at 273 K. For both of the cases, theoretical boundary-layer flow solutions were obtained that incorporate the velocity slip and temperature jump corrections into the boundary conditions. The solutions obtained by the statistical BGK and ES-BGK methods were compared with the slip-flow boundary-layer theory and the benchmark DSMC method. For both of the thermal boundary cases, the shock wave appearing at the leading edge of the plate was captured and the boundary layer was shown to be self-similar. Solutions obtained by the numerical methods agreed well with boundary-layer theory for both of the cases. BGK methods were shown to work well for modeling the compressible flow over a flat plate, and particularly the statistical ES-BGK solutions were shown to be in better agreement with the theoretical and the benchmark DSMC solutions than the BGK ones due to the better physical representation of the gas Prandtl number. In terms of numerical efficiency, the statistical BGK/ES-BGK method was found to be superior to the DSMC method. Based on the presented studies, we are planning a future work to examine a hybrid approach in which the DSMC and BGK methods can be combined to optimize the performance of a multilength scale simulation. Internal as well as external flows through mesoscale devices are one important example of such multilength scale applications. When such devices are used in space applications, the validity and accuracy of the Navier–Stokes equations is questionable, thereby making the use of efficient kinetic approaches imperative.

Acknowledgments

The research being performed at Pennsylvania State University is supported by the U.S. Air Force Office of Scientific Research grant no. F49620-02-1-0104 and is gratefully acknowledged. Special thanks are to M. Ivanov of the Institute of Theoretical and Applied Mechanics, Novosibirsk, Russia, for the use of the original SMILE code. We also acknowledge the fruitful discussions with S.F. Gimelshein of Edwards Air Force Base, California, which helped us implement the statistical BGK scheme using the baseline DSMC SMILE code.

References

[1] Chapman, D., and Rubesin, M., "Temperature and Velocity Profiles in the Compressible Laminar Boundary Layer with Arbitrary Distribution of Surface Temperature," *Journal of the Aeronautical Sciences*, Vol. 16, No. 9, 1949, pp. 547–565.

[2] Cecil, E., and McDaniel, J., "Planar Velocity Measurements of Rarefied Hypersonic Flow over a Tether Using Laser-Induced Iodine Fluorescence," AIAA Paper 2005-4695, 2005.

[3] Ho, C., and Tai, Y., "Micro-Electro-Mechanical Systems (MEMS) and Fluid Flows," *Annual Review of Fluid Mechanics*, Vol. 30, 1998, pp. 579–612. doi:10.1146/annurev.fluid.30.1.579

[4] Liou, W. W., and Fang, Y., *Microfluid Mechanics Principles and Modeling*, Nanoscience and Technology Series, McGraw–Hill, New York, 2006.

[5] Padilla, J., and Boyd, I., "Assessment of Gas-Surface Interaction Models for Computation of Rarefied Hypersonic Flow," *Journal of Thermophysics and Heat Transfer*, Vol. 23, 2009, p. 96. doi:10.2514/1.36375

[6] Sun, Q., and Boyd, I., "Flat-Plate Aerodynamics at Very Low Reynolds Number," *Journal of Fluid Mechanics*, Vol. 502, 2004, pp. 199–206. doi:10.1017/S0022112003007717

[7] Gallis, M., and Harvey, J., "Modeling of Chemical Reactions in Hypersonic Rarefied Flow with the Direct Simulation Monte Carlo Method," *Journal of Fluid Mechanics*, Vol. 312, 1996, pp. 149–172. doi:10.1017/S0022112096001954

[8] Gallis, M., and Harvey, J., "The Modeling of Chemical Reactions and Thermochemical Nonequilibrium in Particle Simulation Computations," *Physics of Fluids*, Vol. 10, 1998, p. 1344. doi:10.1063/1.869660

[9] Yutaka, T., "Multi-Scale Modeling of Dense Phase Gas-Particle Flow," *Chemical Engineering Science*, Vol. 62, 2007, pp. 3410–3418. doi:10.1016/j.ces.2006.12.090

[10] Gallis, M., and Harvey, J., "Atomic Species Radiation from Air Modeled with Direct Simulation Monte Carlo Method," *Journal of*

Thermophysics and Heat Transfer, Vol. 9, 1995, pp. 456–463.
doi:10.2514/3.687

[11] Boyd, I., Phillips, W., and Levin, D., "Prediction of Ultra-Violet Radiation in Nonequilibrium Hypersonic Bow-Shock Waves," *Journal of Thermophysics and Heat Transfer*, Vol. 12, 1998, pp. 38–44.
doi:10.2514/2.6299

[12] Gallis, M. A., and Torczynski, J. R., "The Application of the BGK Model in Particle Simulations," AIAA Paper No. 2000-2360, June 2000.

[13] Andries, P., Bourgat, J., Tallec, P., and Perthame, B., "Numerical Comparison Between the Boltzmann and ES-BGK Models for Rarefied Gases," *Computer Methods in Applied Mechanics and Engineering*, Vol. 191, 2002, pp. 3369–3390.
doi:10.1016/S0045-7825(02)00253-0

[14] Titov, E., Kumar, R., Levin, D., Gimelshein, N., and Gimelshein, S., "Analysis of Different Approaches to Modeling of the Nozzle Flows in the Near Continuum Regime," *26th International Symposium on Rarefied Gas Dynamics*, Springer, New York, July 2008.

[15] Nanbu, K., "On the Simulation Method for the Bhatnagar–Gross–Krook Equation," *Journal of the Physical Society of Japan*, Vol. 50, 1981, pp. 3154–3158.
doi:10.1143/JPSJ.50.3154

[16] Omar, A., Chit, O., Asrar, W., and Ismail, A., "Accuracy of Bhatnagar–Gross–Krook Scheme in Solving Laminar Viscous Flow Problems," *AIAA Journal*, Vol. 47, No. 4, 2009, pp. 885–892.
doi:10.2514/1.35247

[17] Anderson, J., *Hypersonic and High Temperature Gas Dynamics*, McGraw–Hill, New York, 1989.

[18] Burt, J. M., and Boyd, I. D., "Evaluation of a Particle Method for the Ellipsoidal Statistical Bhatnagar–Gross–Kroook Equation," AIAA Paper 2006-989, Jan. 2006.

[19] Bird, G. A., *Molecular Gas Dynamics and the Direct Simulation of Gas Flows*, Clarendon Press, Oxford, 1994.

[20] Ivanov, M., and Gimelshein, S., "Current Status and Prospects of the DSMC Modeling of Near-Continuum Flows of Non-Reacting and Reacting Gases," *Proceedings of the Rarefied Gas Dynamics 23rd International Symposium, American Institute of Physics Conference*, Vol. 663, Springer, New York, 2003, pp. 339–348.

[21] Ivanov, M., and Rogasinsky, S., "Analysis of Numerical Techniques of the Direct Simulation Monte Carlo Method in the Rarefied Gas Dynamics," *Soviet Journal of Numerical Analysis and Mathematical Modelling*, Vol. 3, 1988, pp. 453–465.
doi:10.1515/rnam.1988.3.6.453

[22] Holway, L., "Kinetic Theory of Shock Structure Using Ellipsoidal Distribution Function," *Proceedings of the Fourth International Symposium on Rarefied Gas Dynamics*, Academic Press, New York, 1966, pp. 193–215.

[23] Cercignani, C., *The Boltzmann Equation and its Applications*, Springer–Verlag, New York, 1988.

[24] Kumar, R., Titov, E., and Levin, D., "Reconsideration of Planar Couette Flows Using the Statistical Bhatnagar–Gross–Krook Approach," *Journal of Thermophysics and Heat Transfer*, Vol. 24, No. 2, 2010, pp. 254–262.
doi:10.2514/1.44409

[25] Anderson, J., *Modern Compressible Flow with Historical Perspective*, 3rd ed., McGraw–Hill, New York, 2003.